Plasmonic Nano-Oven by Concatenation of Multishell Photo-Thermal Enhancement

– SUPPORTING INFORMATION –

Lijun Meng,[1,2] Renwen Yu,[1] Min Qiu,[2] and F. Javier García de Abajo[1,3,*]

[1] *ICFO-Institut de Ciencies Fotoniques, The Barcelona Institute of Science and Technology, 08860 Castelldefels (Barcelona), Spain*

[2] *State Key Laboratory of Modern Optical Instrumentation, Zhejiang University, Hangzhou 310027, China*

[3] *ICREA-Institució Catalana de Recerca i Estudis Avançats, Passeig Lluís Companys 23, 08010 Barcelona, Spain*

(Dated: July 23, 2017)

I. OPTIMIZED OPTICAL STRUCTURE VS OPTIMIZED THERMAL STRUCTURE

A structure that is optimized to produce a large average field intensity at its core region is not necessarily optimum to produce a high increase of temperature under external illumination, as we discuss in the main paper. For the simple gold/silica coreshell nanoparticle depicted in Fig. 3a of the main paper, the radii of the optically-optimized structure are R_1 =14 nm and R_2 =17 nm, as shown in Fig. S1a. However, the thermally-optimized structure corresponds to radii R_1 =23 nm and R_2 =28 nm, as shown in Fig. S1b.

II. OPTICAL FIELD ENHANCEMENT IN SILVER-BASED MULTISHELLS

We show in Fig. S2 the electric near-field intensity distributions for a silver/silica coreshell and a $N = 3$ multishell, optimized to render maximum enhancement at a wavelength of 690 nm. The silver/silica interfaces are placed at radial distances of 29 nm and 32 nm in the coreshell, and 5 nm, 8 nm, 13 nm, 16 nm, 42 nm, and 45 nm in the multishell. Compared with the gold/silica structures of Fig. 3 (see main paper), we observe larger intensity enhancement using silver, reaching a maximum $> 10^5$. This $\sim$ 10-fold increase in intensity enhancement when moving from gold to silver is consistent with the $\sim$ 3-fold increase in Drude lifetime τ, and the scaling of the resonance near-field peak intensity as $\propto \tau^2$.

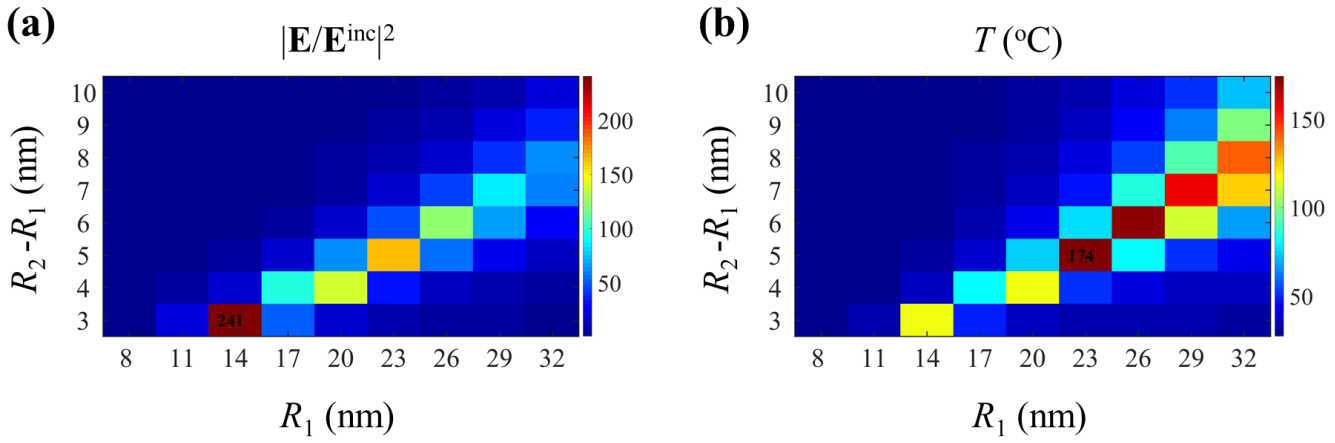

FIG. S1: **Optimization of optical and thermal parameters in a gold/silica coreshell structure. (a)** Average electric field intensity enhancement and **(b)** temperature increase at the core of a nanoparticle like that shown in Fig. 3a of the main paper, as a function of the silica core radius R_1 and the gold shell thickness $R_2 - R_1$. The intensity of the external pump is 1 GW/m^2.

*Electronic address: javier.garciadeabajo@nanophotonics.es

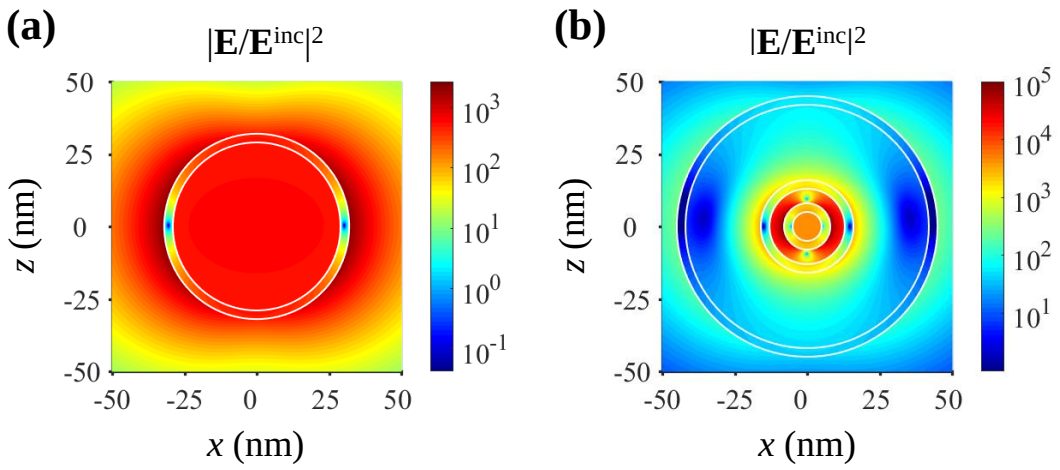

FIG. S2: **Optical field enhancement in silver/silica structures.** We show the electric near-field intensity distribution at a wavelength of 690 nm for two optimized airborne structures: a coreshell (a) and a multishell consisting of 3 silver layers (b).

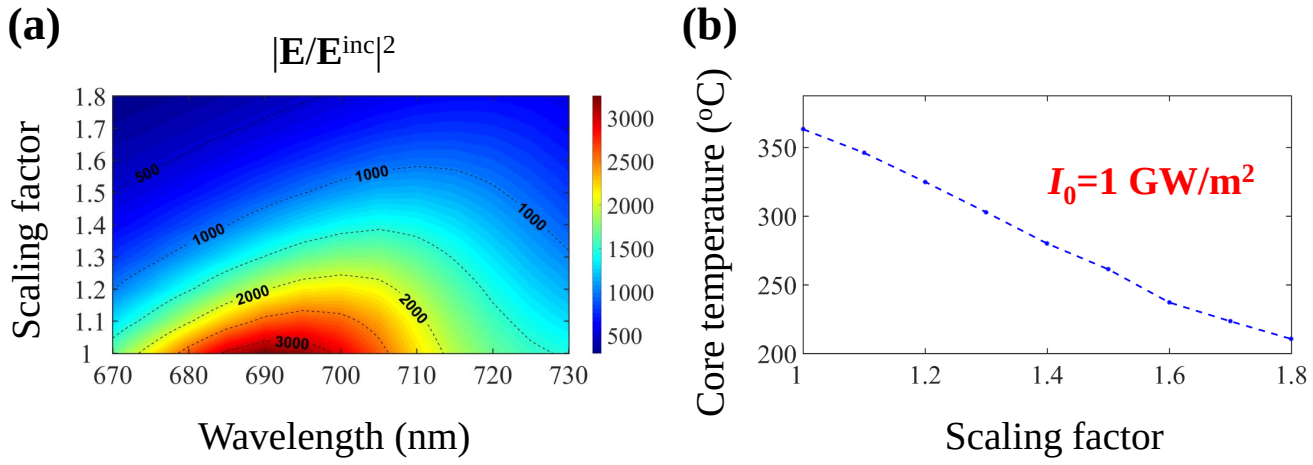

FIG. S3: **Dependence of the optical and thermal performances on particle size. (a)** Electric-field-intensity enhancement averaged over the volume of the central silica core for nano-ovens like the one shown in Fig. 4c of the main paper, with all radii multiplied by a common scaling factor (vertical axis). **(b)** Temperature increase at the center of the nano-oven as a function of the scaling factor under an external pump intensity of 1 GW/m^2, tuned to the scaling-factor-dependent wavelength for which the enhancement is maximum.

III. SIZE DEPENDENCE OF THE ELECTRIC FIELD ENHANCEMENT AND TEMPERATURE INCREASE

We study in Fig. S3 the influence of the nano-oven geometrical parameters on its average field-intensity enhancement over the volume of the central silica core. More specifically, all the geometrical parameters of the nano-oven shown in Fig. 4c are scaled by a common factor ranging from 1 to 1.8. As the scaling factor increases, the resonance wavelength redshifts and the maximum value of the enhancement decreases. As a result, the temperature in the center of the nano-oven also decreases, even though the wavelength is tuned to the maximum value for each scaling factor.

IV. OPTICAL AND THERMAL PROPERTIES OF ALUMINUM-BASED NANO-OVENS

We present in Fig. S4 a similar study as in Fig. 3 of the main paper, but replacing gold by aluminum, and considering a new resonant incident light wavelength of 300 nm. We conclude that the field enhancements in the aluminum multishells are much weaker than those of their gold counterparts (cf. Figs. S4 and 3). Additionally, we

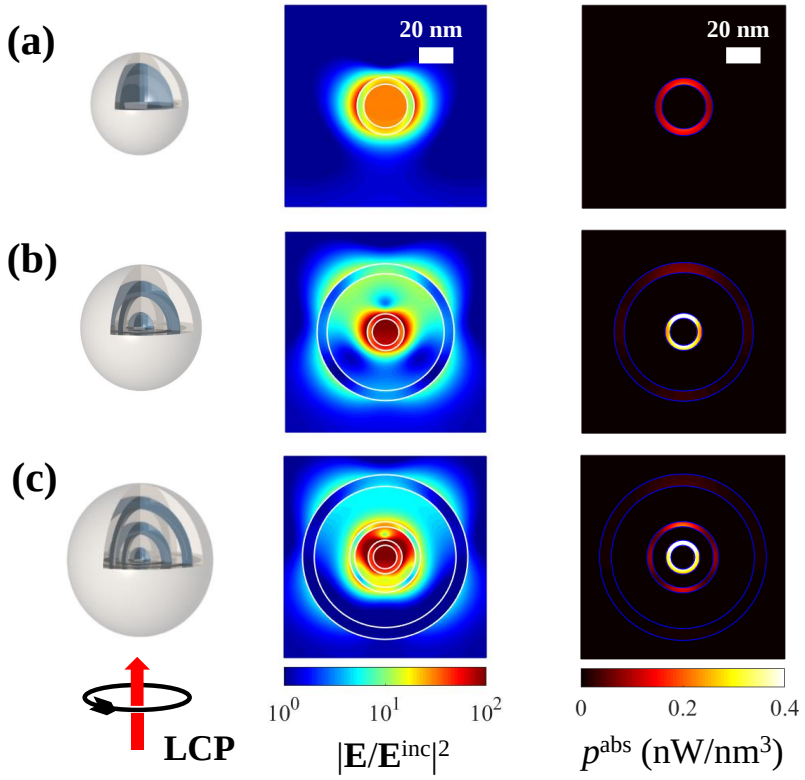

FIG. S4: **Optical and thermal properties of aluminum-based nano-ovens.** We show results for optimized nanoparticles with single (a), double (b), and triple (c) aluminium shells for the same geometrical parameters as in Fig. 4d-f of the main paper. In each row, we show from left to right a scheme of the nanoparticle, the electric near-field intensity distribution under plane-wave illumination at a wavelength of 300 nm, and the absorption power density p^{abs} generated at the same wavelength with a pump intensity of $1\,\mathrm{GW/m^2}$.

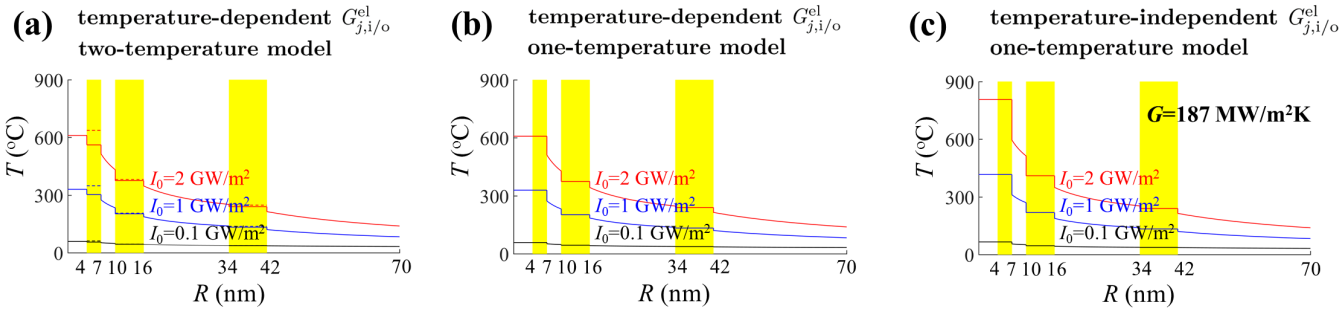

FIG. S5: **Model dependence of the calculated temperature profiles.** We show calculated temperature profiles under different external pump intensities (see labels) for a gold/silica nano-oven using different models: **(a)** two-temperature model with temperature-dependent electron-lattice TBCs $G^{\mathrm{el}}_{j,\mathrm{i/o}}$ at the gold-silica interfaces (this panel is the same as Fig. 4c of the main paper); **(b)** one-temperature model (i.e., the electron and lattice temperatures are set equal in the metal regions) with temperature-dependent electron-lattice TBCs; **(c)** one-temperature model with a temperature-independent total TBCs $G^{\mathrm{el}}_{j,\mathrm{i/o}} + G^{\mathrm{ll}}_{j,\mathrm{i/o}} = 187\,\mathrm{MW\,m^{-2}\,K^{-1}}$.

find that both the central and outer aluminum shells operate more actively on the quadrupole modes, rather than the dipole modes. Because the TBC of aluminum/silica interfaces is relatively larger, the temperature variations at multiple interfaces play a smaller role, so a bigger structure (no longer subwavelength) containing thicker dielectric shells would be needed to optimize the thermal performance.

V. DEPENDENCE ON THERMAL DISSIPATION MODEL

We explore in Fig. S5 two details of the thermal dissipation model: the assumption of two different temperatures in the electron and lattice systems of the metal; and the temperature dependence of the electron-lattice TBCs in the metal/dielectric interfaces. In all of the results presented in the rest of the figures within this work, we assume this two-temperature model for the metal, as well as temperature-dependent electron-lattice TBCs. This leads to the results reproduced in Fig. S5a for a gold/silica nano-oven under different pump intensities (copied from Fig. 4c of the main paper).

In Fig. S5b we present results from a one-temperature model, obtained by setting the electron and lattice temperatures equal in the metal (i.e., $T_j^{\mathrm{e}} = T_j^{\mathrm{l}}$), so that Eq. (5) of the main paper is dismissed and Eq. (4) becomes

$$P_j = \left(G_{j,\mathrm{i}}^{\mathrm{el}} + G_{j,\mathrm{i}}^{\mathrm{ll}}\right) S_{j,\mathrm{i}}(T_j^{\mathrm{l}} - T_{j,\mathrm{i}}^{\mathrm{d}}) + \left(G_{j,\mathrm{o}}^{\mathrm{el}} + G_{j,\mathrm{o}}^{\mathrm{ll}}\right) S_{j,\mathrm{o}}(T_j^{\mathrm{l}} - T_{j,\mathrm{o}}^{\mathrm{d}}),$$

(i.e., the first term in the right-hand side of Eq. (4) is replaced by the right-hand side of Eq. (5)). The two- and one-temperature models lead to similar temperature profiles (cf. Figs. S5a and S5b), and in particular, they predict a similar increase in temperature at the core region.

Finally, because the experimental determination of TBCs is sensitive to sample preparation [1] and interfacial imperfections [2], possibly leading to smaller TBCs than those assumed in this work, we analyze in Fig. S5c the effect of eliminating the temperature dependence in $G_{j,\mathrm{i/o}}^{\mathrm{el}}$ by making these coefficients equal to a constant value, so that the total TBCs are given by $G_{j,\mathrm{i/o}}^{\mathrm{el}} + G_{j,\mathrm{i/o}}^{\mathrm{ll}} = 187\,\mathrm{MW\,m^{-2}\,K^{-1}}$, taken from Ref. [3]. Using this assumption together with the one-temperature model, a higher increase in temperature is predicted at the core region, as shown in Fig. S5c, although the effect is not dramatic.

Supplementary References

[1] O. Käding, H. Skurk, and K. Goodson, Appl. Phys. Lett. **65**, 1629 (1994).
[2] P. E. Hopkins, ISRN Mech. Eng. **2013**, 682586 (2013).
[3] X. Chen, Y. Chen, M. Yan, and M. Qiu, ACS Nano **6**, 2550 (2012).